Computation of Low-Density Supersonic Flow over a Pitot Tube

Michael C. Cline,* Jack C. Hyde,† and Richard A. Gentry‡
Los Alamos National Laboratory, Los Alamos, New Mexico

The internal and external flow of N_2 gas over a Pitot tube in the transitional regime between continuum and free-molecular flow is computed using the Navier-Stokes equations. Both slip and no-slip boundary conditions, as well as two different Reynolds numbers, are considered. These numerical solutions illustrate many interesting features of flow in this regime and, in general, are in reasonably good agreement with experiment.

Nomenclature

a = speed of sound
d = Pitot tube inside diameter
D = Pitot tube outside diameter
k = coefficient of thermal conductivity
Kn = Knudsen number
$Kn_{s,d}$ = λ_s/d
$Kn_{s,D}$ = λ_s/D
M = Mach number
n = direction normal to the wall
p = pressure
Pr = Prandtl number
R = gas constant
Re = Reynolds number
$Re_{s,d}$ = $\rho_\infty u_\infty d/\mu_s$
$Re_{s,D}$ = $\rho_\infty u_\infty D/\mu_s$
$Re_{p,d}$ = $Re_{s,d}\sqrt{\rho_s/\rho_\infty}$
$Re_{p,D}$ = $Re_{s,D}\sqrt{\rho_s/\rho_\infty}$
t = time
T = temperature
u = velocity component in the x direction
u_N = velocity component normal to the wall
u_T = velocity component tangent to the wall
v = velocity component in the y direction
x = coordinate direction along the Pitot tube axis
y = coordinate direction along the Pitot tube radius
γ = ratio of specific heats
ϵ = 0 for planar geometry and 1 for axisymmetric geometry
λ = second coefficient of viscosity
λ_s = mean free path based on the stagnation temperature behind the shock
λ_w = mean free path based on the temperature at the wall
μ = first coefficient of viscosity
ρ = density

Subscripts

w = wall
∞ = freestream static conditions
s = stagnation conditions behind the shock

Introduction

PITOT tubes or impact probes are used to determine impact pressure, which then can be used to determine velocity for a wide range of applications. For high-density continuum flows, Pitot tube measurements along with normal shock wave theory produce good results. For extremely low-density free-molecular flows, Pitot tube measurements along with kinetic theory also produce good results. However, for low-density flows in the transitional regime between continuum and free-molecular flow, results are not nearly as reliable. Pitot tubes in this flow regime have been studied experimentally by many investigators (for a survey of these experiments, see Refs. 1 and 2). Although these experiments have produced much useful data, they have not provided the detailed description of the flow that is possible with a theoretical solution.

Therefore the authors used the VNAP2 code,[3] which numerically solves the Navier-Stokes equations, to analyze the flow over and inside a Pitot tube in the transitional regime between continuum and free-molecular flow. Both slip and no-slip boundary conditions are investigated. The flow is assumed to be in thermal equilibrium. A similar approach has been successfully used for flow over a flat plate.[4] In addition, solutions of the Navier-Stokes equations, assuming local similarity, have been generated for flow over a sphere.[5]

Flow Description

The flow geometry is shown in Fig. 1. The computational boundary is denoted by the dashed line. The Pitot tube is denoted by the shaded area. The flow enters from the left and exits at the top right. Because the Pitot tube is circular in cross section the flow is assumed to be axisymmetric. The computation grid corresponding to Fig. 1 is shown in Fig. 2. This grid was used in all computations presented here.

Three separate cases were computed. All cases consisted of Mach 4.0 flow of N_2 gas. The upstream stagnation temperature and the temperature of the Pitot tube were 300 K for all cases. Case 1 has an upstream stagnation pressure of 1.64 kPa. These values produced Reynolds and Knudsen numbers, behind the shock, of 10.0 and 0.058, respectively. See Table 1 for description of the Reynolds and Knudsen

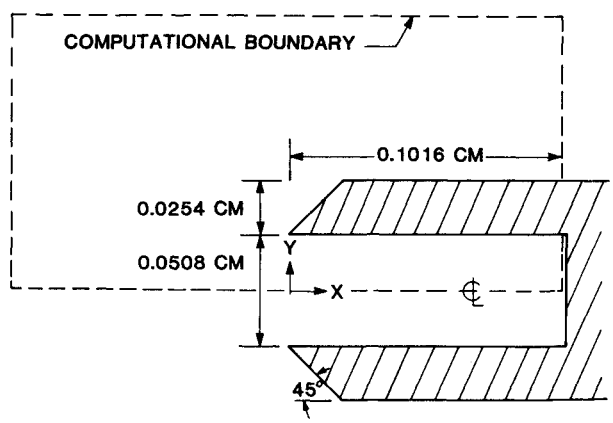

Fig. 1 Flow geometry.

Presented as Paper 85-1032 at the AIAA 20th Thermophysics Conference, Williamsburg, VA, June 19-21, 1985; revision received Nov. 10, 1985.

*Group T-3 Staff Member. Member AIAA.
†Group T-3 Staff Member; currently at Aerojet Tech Systems, Sacramento, CA.
‡Group T-3 Staff Member.

numbers used here. No-slip boundary conditions were employed at the Pitot tube surface. Case 2 differed from case 1 in that slip boundary conditions were used. Case 3 differed from case 2 in that the upstream stagnation pressure was 0.37 kPa, which produced Reynolds and Knudsen numbers, behind the shock, of 2.25 and 0.26, respectively.

Flow Model

Governing Equation

In low density and therefore low Reynolds number flows, viscous effects are important throughout the flowfield. Therefore such simplifying assumptions as those involved in the viscous boundary layer/inviscid external flow model are not appropriate. In addition, the neglect of streamwise viscous effects, as done in the parabolic and thin-layer Navier-Stokes equation models, would also appear to be questionable. For these reasons, we solved the full two-dimensional, time-dependent, compressible Navier-Stokes equations for an ideal gas in thermal equilibrium. These equations are

$$\frac{\partial \rho}{\partial t}+u\frac{\partial \rho}{\partial x}+v\frac{\partial \rho}{\partial y}+\rho\left(\frac{\partial u}{\partial x}+\frac{\partial v}{\partial y}+\frac{\epsilon v}{y}\right)=0 \tag{1}$$

$$\frac{\partial u}{\partial t}+u\frac{\partial u}{\partial x}+v\frac{\partial u}{\partial y}+\frac{1}{\rho}\frac{\partial p}{\partial x}=\frac{1}{\rho}\frac{\partial}{\partial x}\left[(\lambda+2\mu)\frac{\partial u}{\partial x}+\lambda\frac{\partial v}{\partial y}\right]+\frac{1}{\rho}\frac{\partial}{\partial y}\left[\mu\left(\frac{\partial v}{\partial x}+\frac{\partial u}{\partial y}\right)\right]+\frac{\epsilon}{\rho y}\left[(\lambda+\mu)\frac{\partial v}{\partial x}+\mu\frac{\partial u}{\partial y}+v\frac{\partial \lambda}{\partial x}\right] \tag{2}$$

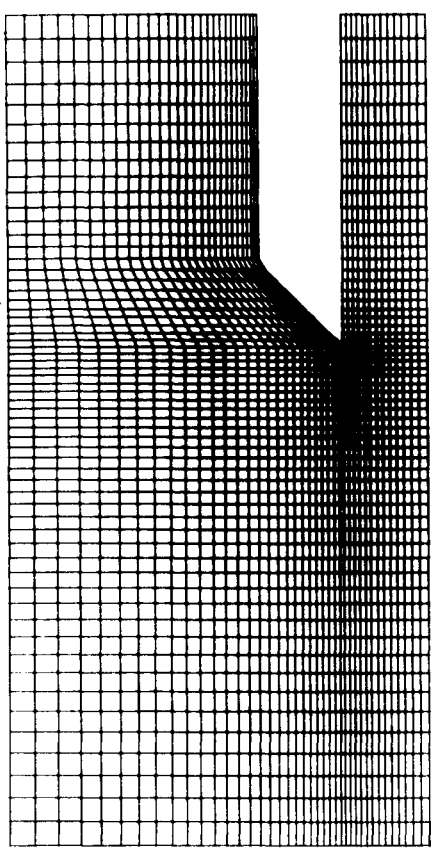

Fig. 2 Computational grid.

$$\frac{\partial v}{\partial t}+u\frac{\partial v}{\partial x}+v\frac{\partial v}{\partial y}+\frac{1}{\rho}\frac{\partial p}{\partial y}=\frac{1}{\rho}\frac{\partial}{\partial y}\left[(\lambda+2\mu)\frac{\partial v}{\partial y}+\lambda\frac{\partial u}{\partial x}\right]+\frac{1}{\rho}\frac{\partial}{\partial x}\left[\mu\left(\frac{\partial v}{\partial x}+\frac{\partial u}{\partial y}\right)\right]+\frac{\epsilon}{\rho y}\left[(\lambda+2\mu)\left(\frac{\partial v}{\partial x}-\frac{v}{y}\right)+v\frac{\partial \lambda}{\partial y}\right] \tag{3}$$

$$\frac{\partial p}{\partial t}+u\frac{\partial p}{\partial x}+v\frac{\partial p}{\partial y}-a^2\left(\frac{\partial \rho}{\partial t}+u\frac{\partial \rho}{\partial x}+v\frac{\partial \rho}{\partial y}\right)=(\gamma-1)\left\{(\lambda+2\mu)\left[\left(\frac{\partial u}{\partial x}\right)^2+\left(\frac{\partial v}{\partial y}\right)^2\right]+\mu\left[\left(\frac{\partial v}{\partial x}\right)^2+\left(\frac{\partial u}{\partial y}\right)^2\right]+2\lambda\frac{\partial u}{\partial x}\frac{\partial v}{\partial y}+2\mu\frac{\partial v}{\partial x}\frac{\partial u}{\partial y}+\frac{\partial}{\partial x}\left(k\frac{\partial T}{\partial x}\right)+\frac{\partial}{\partial y}\left(k\frac{\partial T}{\partial y}\right)+\frac{\epsilon}{y}\left[(\lambda+2\mu)\frac{v^2}{y}+2\lambda v\left(\frac{\partial u}{\partial x}+\frac{\partial v}{\partial y}\right)+k\frac{\partial T}{\partial y}\right]\right\} \tag{4}$$

and

$$p=\rho RT \tag{5}$$

Equation (1) is the conservation of mass or continuity equation; Eqs. (2) and (3) are the x and y momentum equations, respectively; and Eq. (4) is the internal energy equation written in terms of pressure, using the equation of state for a perfect gas, Eq. (5). The steady-state flow, when it exists, is the transient solution for large time. The flow is assumed to be laminar. The fluid is N_2 and is considered to be an ideal gas with a constant $\gamma=1.4$. The coefficients of viscosity μ and thermal conductivity k are

$$\mu=1.25\times10^{-7}T^{0.87}\,(Pa-s) \tag{6}$$

$$k=1.71\times10^{-4}T^{0.87}\,(W/m-K) \tag{7}$$

The second coefficient of viscosity, λ, was set equal to $-2\mu/3$. To stabilize these calculations in the bow shock wave region, an explicit artificial viscosity, based on the velocity gradient, was added to the molecular values. For additional details see Ref. 3.

Boundary Conditions

The left computational boundary in Fig. 1 is a supersonic inflow boundary, and so all flow variables are specified and held fixed with respect to time. The lower boundary is the flow centerline, or axis of symmetry. The right lower boundary is the closed end of the Pitot tube, where the velocity components u and v are set to zero and the temperature is set equal to the wall value. The right upper boundary is an outflow boundary and the flow variables are extrapolated from the values at the interior grid points. The upper boundary can be either an inflow or an outflow boundary. If the flow across this boundary is downwared (inflow), then the freestream values of the u velocity component, the pressure p, and the density ρ are specified. If the flow is upward (outflow), then only the freestream value of p is specified.

Table 1 Reynolds and Knudsen numbers

Case	$Re_{s,d}=\rho_\infty u_\infty d/\mu_s$	$Re_{s,D}$	$Re_{p,d}=Re_{s,d}\sqrt{\rho_s/\rho_\infty}$	$Re_{p,D}$	$Kn_{s,d}=\lambda_s/d$	$Kn_{s,D}$
1 and 2	10.0	20.0	22.4	44.8	0.058	0.029
3	2.25	4.5	5.0	10.0	0.26	0.13

There are two sets of boundary conditions used on the Pitot tube solid wall. The first is the no-slip/specified wall temperature condition, which can be written as

$$y=y_w:\ u=v=0, \qquad T=T_w \tag{8}$$

where the subscript w denotes the wall value. This condition will be called the no-slip condition. The second is the velocity slip/temperature jump condition, which can be written as

$$y=y_w:\ u_T=\lambda_w\left(\frac{\partial u_T}{\partial n}\right)_w, \qquad u_N=0$$

$$T=T_w+\frac{2\gamma\lambda_w}{(\gamma+1)Pr}\left(\frac{\partial T}{\partial n}\right)_w \tag{9}$$

where λ_w denotes the mean free path at the wall, Pr is the Prandtl number, u_T denotes the velocity tangent to the wall, u_N the velocity normal to the wall, and n the direction normal to the wall. All accommodation coefficients are assumed to be unity. This second condition will be referred to as the slip condition.

Other forms of the velocity slip/temperature jump boundary conditions were not investigated in the present study. Jain[6] stated that different conditions have little effect on the pressure field.

Numerical Method

The interior grid points in the VNAP2 code were computed using the unsplit MacCormack scheme.[7] In order to improve the computational efficiency for these low Reynolds number flows, local or variable time steps were employed. In this procedure, the time step at a grid point is the local maximum allowable value and, therefore, is not constant at all grid points. This produces a transient solution that is not time accurate but, rather, converges to steady state 5-10 times faster than the standard constant time step method.

All unspecified boundary grid point values were calculated using a characteristic scheme. The gradients used in the slip boundary conditions were evaluated using one-sided, first-order differences. For further details on the VNAP2 code see Ref. 3.

The computational grid is shown in Fig. 2. The grid was refined in the y direction near the Pitot tube walls to resolve the viscous boundary layers. In addition, the grid was refined in both the x and y directions near the leading edge to resolve the stagnation region. However, the grid was not redefined in the x direction near the right end of the Pitot tube because the flow gradients in this region are very small. A grid with spacings adjacent to the Pitot tube that were twice as fine as the present values was also used for case 1, the case requiring the finest grid, producing very similar results.

Results

The Mach number and pressure contours for cases 1 through 3 are shown in Figs. 3 and 4, respectively. Looking at the top two frames of Figs. 3 and 4, it is seen that the effect of slip is mainly in the region adjacent to the external surface of the Pitot tube. This is further illustrated by the external velocity and temperature profiles for cases 1-3, as shown in Figs. 5 and 6, respectively. Because of the low velocities, there are few internal effects as a result of the slip boundary condition.

Referring to the second and third frames in Fig. 3, it is seen that the decrease in Reynolds number significantly increases the shock thickness. However, from Fig. 4, it is seen that the pressure rise is concentrated very close to the Pitot tube. This occurs because the Navier-Stokes equations contain velocity and temperature diffusion terms, but not pressure and density diffusion terms. Therefore, as the Reynolds number decreases, the temperature and therefore the ratio p/ρ diffuse out, but not necessarily p and ρ. Figures 5 and 6 show that the

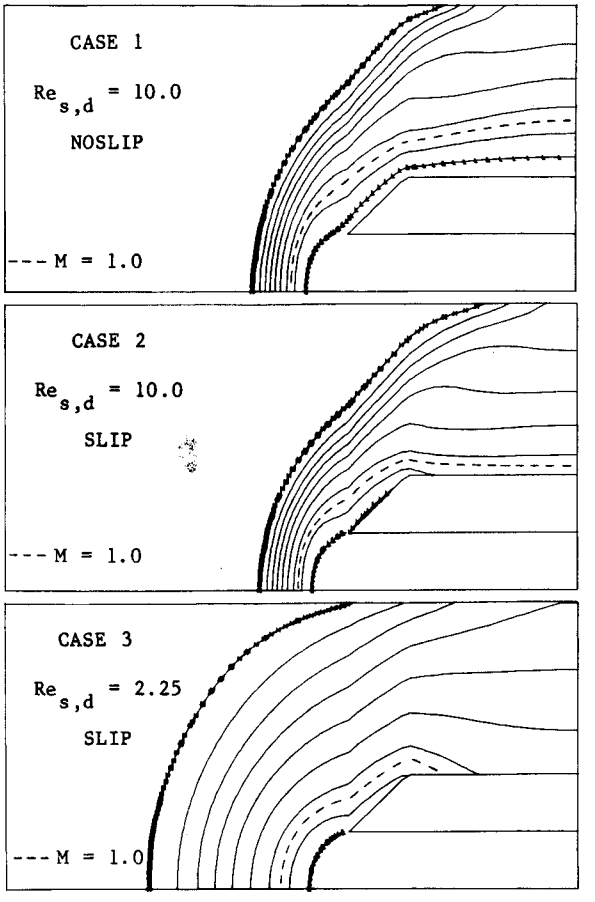

Fig. 3 Mach number contours for cases 1-3.

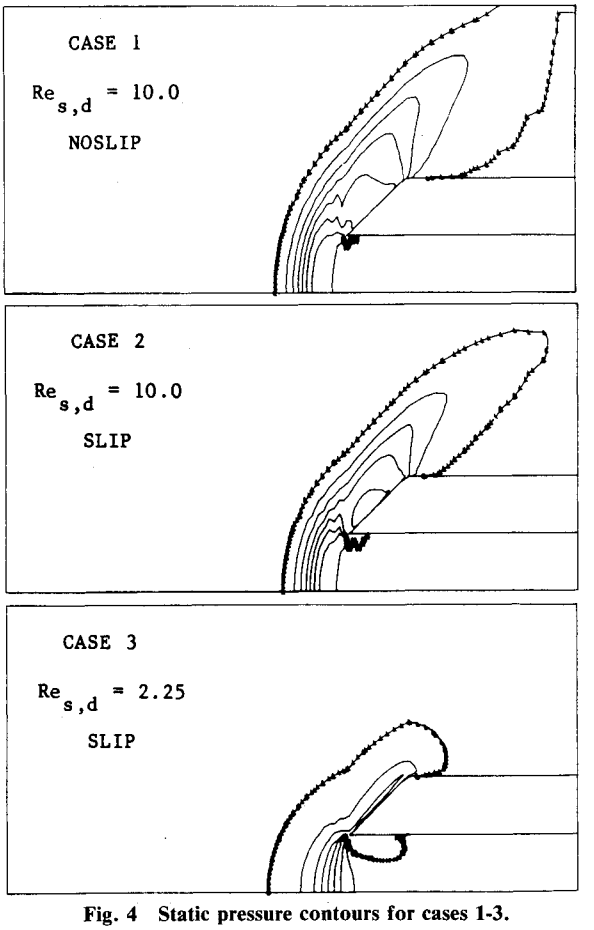

Fig. 4 Static pressure contours for cases 1-3.

slip velocity and temperature jump increase as the Reynolds number is decreased. The external slip velocity and temperature jump as a function of x are shown in Fig. 7.

Streamline plots for cases 1-3 are shown in Fig. 8. From Fig. 8 it is seen that a ring vortex stands at the entrance of the Pitot tube. The initial location of the streamlines in the ring vortex were arbitrarily selected to help visualize the vortex and do not represent flow gradients. The velocities in the ring vortex were about two orders of magnitude less than the upstream values. The static pressure along the Pitot tube centerline, for cases 1-3, is shown in Fig. 9. From Fig. 9 it is seen that at the lower Reynolds number more of the pressure rise occurs inside the Pitot tube. The ratio of the stagnation presure p_T to the ideal Rayleigh Pitot tube formula value p_{TI} for both the present theoretical values at the right end of the tube and the experimental values of Ref. 1 are shown in Fig. 10. One ques-

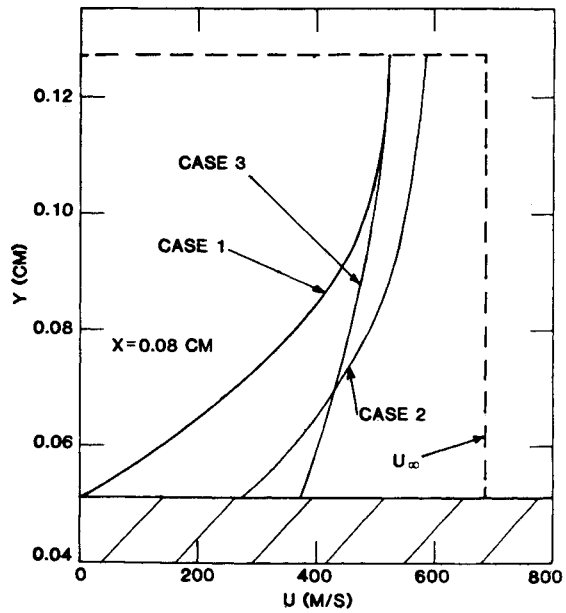

Fig. 5 External flow velocity profiles for cases 1-3.

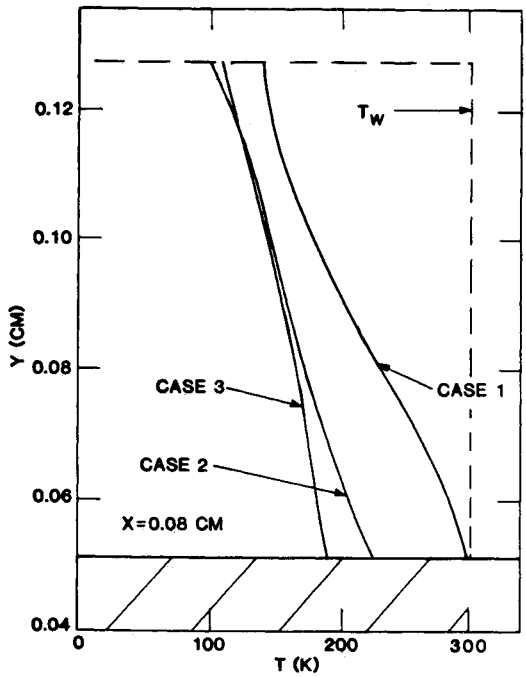

Fig. 6 External static temperatures profiles for cases 1-3.

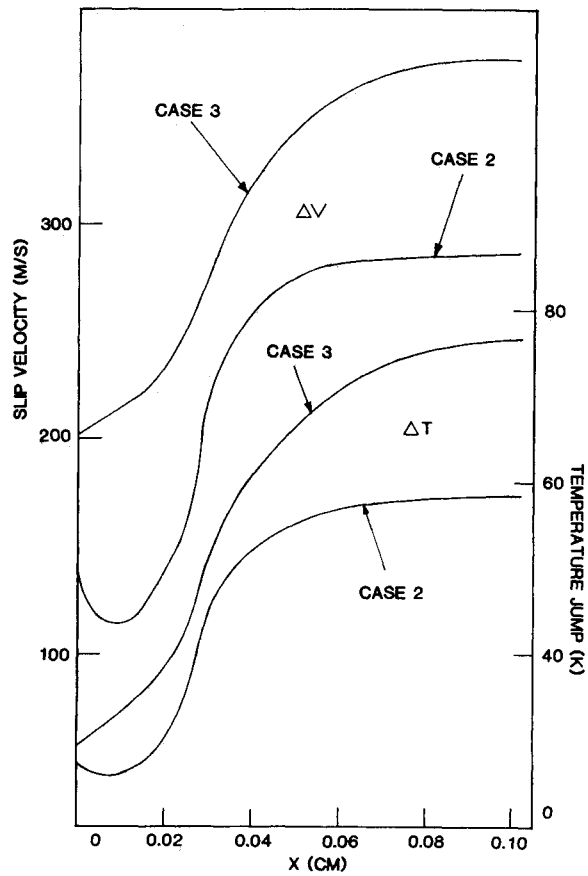

Fig. 7 External slip velocity and temperature jump as a function of x for cases 2 and 3.

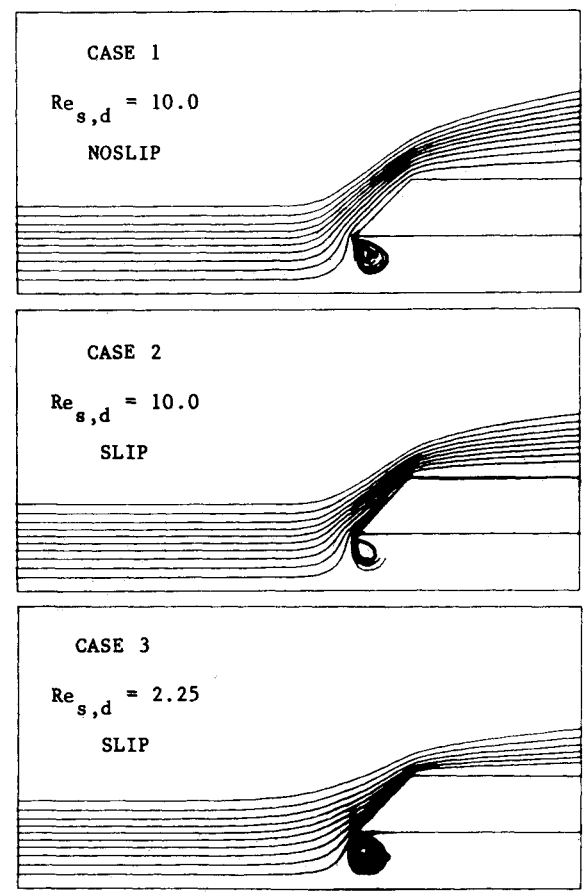

Fig. 8 Streamline plots for cases 1-3.

tion, in comparing the computed solution with the experimental data, concerns which diameter to use in the Reynolds number. A comparison of the two different Pitot tube tip configurations used here and in Ref. 1 is shown in Fig. 11. It appears that the internal diameter, which is the present tip diameter, may be more appropriate. From Fig. 10 we see that using the inside diameter gives better agreement with experiment. Cases 1 and 2 agree very well with experiment, whereas the pressure for case 3 is somewhat higher than that of the experiment. This could be due to either the different geometries, as shown in Fig. 11, or the continuum flow assumption of the Navier-Stokes equations, which tends to underpredict the shock thickness and thus overpredict the pressure behind the shock. Additional calculations with different geometries and at several different Reynolds numbers are required to explain this difference.

A comparison of the theoretical shock thickness[8] and experimentally determined standoff distance[9] with the present Mach number contours is shown in Fig. 12. From Fig. 12 it is seen that there is good agreement for case 2; however, for case 3, the present results appear to produce a smaller shock thickness than the results of Ref. 8. It is not clear what causes this difference, because the shock thickness of Ref. 8 is also based on a solution of the Navier-Stokes equations. The present results appear to produce a shock standoff distance that is larger than that of Ref. 9. This may be due to the fact that the results in Ref. 9 are not given as a function of Reynolds number. Also, these results are for a flat-faced, circular cylinder. Here again, it is not clear which diameter of the Pitot tube is the more appropriate. The external diameter produced data in better agreement with Ref. 9 and was therefore used.

The two high Reynolds number cases exhibited an oscillatory cavity pressure and shock location as the flow evolved to steady state. The amplitude of this oscillation appeared to decrease with time. Because of this and the fact that the flow was not time accurate, owing to the use of local time steps, the solution was time averaged over the oscillation wavelength to speed up the convergence to steady state. The lower Reynolds number case did not appear to exhibit this behavior over the time interval investigated.

The computational times for these calculations are rather lengthy owing to the long propagation time of the viscous ef-

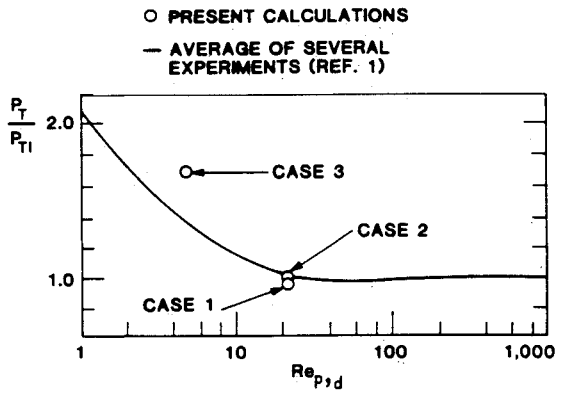

Fig. 10 Comparison of the theoretical and experimental ratios of stagnation pressure p_T to the ideal Rayleigh Pitot tube formula value p_{TI}.

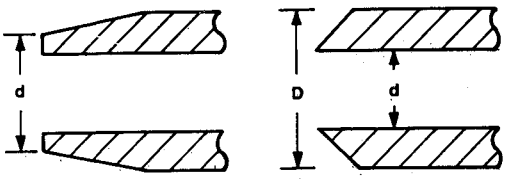

Fig. 11 Comparison of the Pitot tube tip configurations used here (right) with that of Ref. 1.

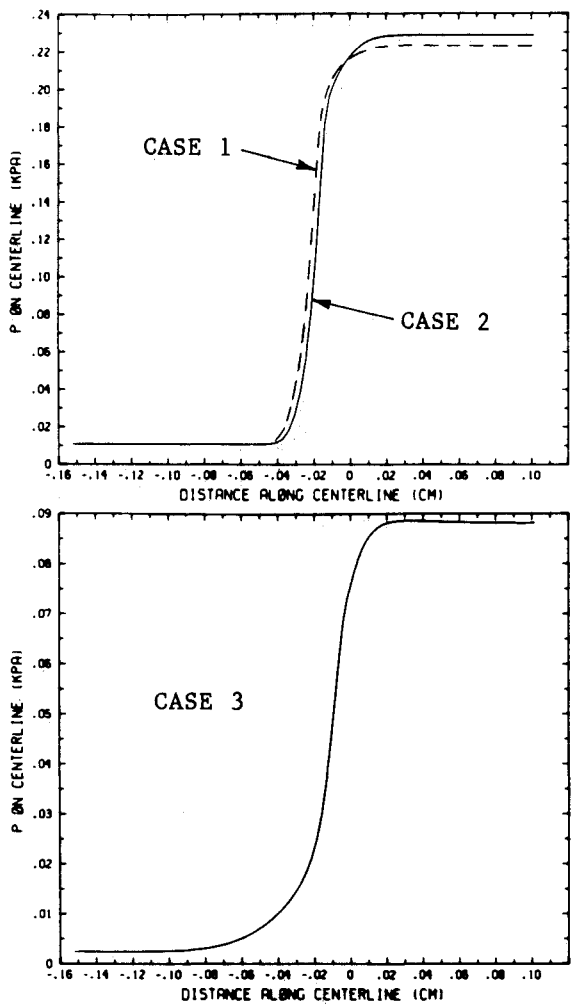

Fig. 9 Static pressure along the centerline for cases 1-3.

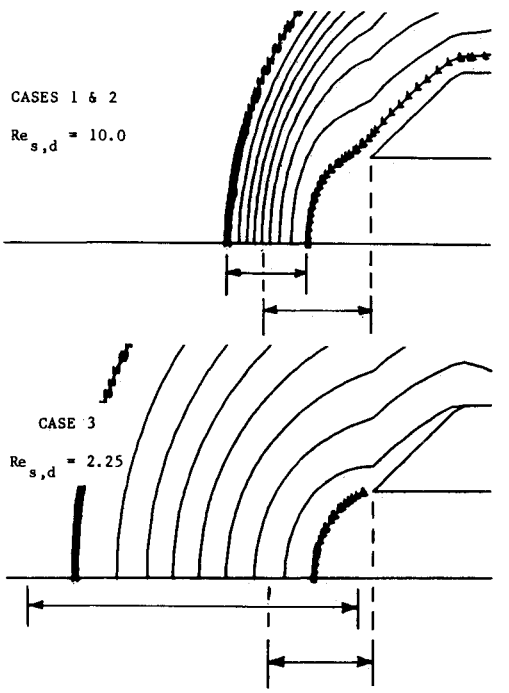

Fig. 12 Comparison of the shock thickness from Ref. 8 and the standoff distances from Ref. 9 with the computed Mach number contours for cases 1-3.

fects. Cases 1 and 2 required about 1 h of CPU time on a Cray 1, while case 3 required 4 h. The CPU time for case 3 could be reduced by noting that a coarser grid could adequately resolve the flow at this lower Reynolds number. These times could also be reduced by using an implicit treatment of the viscous terms in the Navier-Stokes equations. However, because increased numerical diffusion is usually a consequence of implicit schemes operating at very large time steps, one must proceed carefully so as not to destroy the molecular diffusion effects.

Conclusions

Numerical solutions to the full Navier-Stokes equations for the internal and external flow of N_2 gas over a Pitot tube have been presented. These solutions show that details of such flows and the effects of slip vs no-slip boundary conditions, as well as the effect of Reynolds number. In general, these results are in reasonably good agreement with experiment.

The results show that the Navier-Stokes equations apply above Reynolds numbers $Re_{s,d}$ of 10.0, but additional calculations are required to determine their applicability as the Reynolds number approaches unity. The rather lengthy computational times indicate that a more efficient treatment of the viscous terms is desirable.

Acknowledgments

This work was supported by the U.S. Department of Energy. The authors wish to thank Professor Sam S. Fisher of the University of Virginia for his assistance.

References

[1]Fisher, S.S., "The Effect of Rarefaction on Impact Pressure Measurements in Supersonic Flows," *Proceedings of the 13th International Symposium on Rarefied Gas Dynamics,* Novosibirsk, USSR, July 1982.

[2]Fisher, S.S., Yurkanin, D.J., Graybeal, G.A., and Scott, J.E. Jr., "Measurements of the Impact Probe Rarefaction Effect in High Mach Number $\gamma = 7/5$ CO_2 Flows," *Proceedings of the 14th International Symposium on Rarefied Gas Dynamics,* Tsukuba Science City, Japan, July 1984.

[3]Cline, M.C., "VNAP2: A Computer Program for Computation of Two-Dimensional, Time-Dependent, Compressible, Turbulent Flow," Los Alamos National Laboratory, Los Alamos, NM, Rept. LA-8872, Aug. 1981.

[4]Butler, T.D., "Numerical Solutions of Hypersonic Sharp-Leading-Edge Flows," *Physics of Fluids,* Vol. 10, June 1967, pp. 1205-1215.

[5]Jain, A.C. and Adimurthy, V., "Hypersonic Merged Stagnation Shock Layers Parts I and II," *AIAA Journal,* Vol. 12, March 1974. pp. 342-354.

[6]Jain, A.C., personal communication, Williamsburg, VA, June 1985.

[7]MacCormack, R.W., "The Effect of Viscosity in Hypervelocity Impact Cratering," AIAA Paper 69-354, April 1969.

[8]White, F.M., *Viscous Fluid Flow,* McGraw-Hill Book Co., New York, 1974, pp. 195-200.

[9]Liepmann, H.W. and Rosko, A., *Elements of Gasdynamics,* John Wiley & Sons, New York, 1957, pp. 103-106.